On trapeze wing aerodynamics calculations based on improved vortex lattice method

JACOB NAGLER
NIRC,
Haifa, Givat Downes, ISRAEL

Abstract: This paper presents, aerodynamics coefficients calculation (Lifting & drag coefficients, pressure central location) of Trapeze wing shape configurations for different aspect ratios (ARs) values by using improved vortex lattice method (VLM), compared with finite-wing and slender body theories. The planar wing was divided into N panels of the size: 6X6 with trapezoid shape panels. As expected, for high ARs the VLM solution for the lifting coefficient is coincided with the finite wing theory whereas for small ARs (<1) it is coincided with the slender body theory (~1). Afterwards, we obtained that the calculated VLM induced drag becomes closer to the finite-wing theory as the AR value is increased.

Key-words: VLM; finite wing; slender body; leading edge suction force;

Received: June 14, 2021. Revised: January 15, 2022. Accepted: March 4, 2022. Published: April 13, 2022.

1 Introduction

In this current study, VLM (Vortex lattice method) theory is applied on Trapeze wing shape configurations for different aspect ratios (ARs) values by using improved vortex lattice method (VLM), compared with finite-wing and slender body theories. This study continues the previous author study and VLM model [1] by improving it, using the leading edge suction analogy that considers the suction force and explains analytically the vortex-lift theory. In the past the leading edge suction analogy was proposed by Polhamus [2, 3], applied on Delta wings, and later extended by Traub [4]. Advanced numerical analysis of aerodynamics properties due to wing geometry shape and different geometry wing angles that includes different geometry manipulations in order to achieve the optimal aerodynamic flight have been studied over the two decades. For instance, studies concerning swept and semi-slender wings for blunt leading edge shape [5], flap and aileron deflection [6], flapping wings in a hover [7], various leading edge shape [8, 9], morphing wings [10] and recently non-slender delta wings [11] have been studied. Finally, classic experimental and theoretical work was performed over the years by [12-16].

2 Improved VLM analytic model

The improved model [30] includes the calculated suction coefficient (based on Fig. 2) as:

$$C_T = \frac{\rho \sum_k \left(U\alpha + \omega\right)\Big|_k \Gamma_k \Delta y_k}{qs} \quad (1)$$

while the wing perpendicular velocity generates an axial force which is the leading edge suction force. Note that according to Katz & Plotkin [17], the calculation is only considering the cells trailing vortices without their bound vortex. Additionally, according to Moran [18] for specific cell along with the symmetric cell in the other side – the calculation only considers the trailing vortices, similarly to Katz & Plotkin [17]. However, according to Moran [18], the other cells should be considering all the other vortices. Similar way, appears in Margason & Lamar [19]. Since we concern here a trapezoidal wing geometry shape; then the attack and flow leading edges are located on straight lines, therefore the adjacent vortices of all the cells in the whole framework are located along the projection wingspan. In other words, an adjacent vortex will contribute infinity induced velocity on each cell located further along the projection wingspan such as singularity is obtained using methods [18, 19]. Although method [17] might be used (no-singularity), however, inaccuracy might be generated due to the negligence the adjacent vortices. Hence, we will use a different method, based on induced velocity calculation on each cell, only the adjacent vortices will be calculated without the vortices located on the same straight line such as accurate improved calculation will be resulted for [17].

Next, measuring length chord and calculating wing trapezoid surface area, averaged aerodynamic chord together with rearward sweep angle, we have obtained the following geometrical parameters:

$$b = \frac{AR}{2}\left(c_{root} - c_{tip}\right), S_w = \frac{b^2}{AR}, \bar{\Lambda} = \tan^{-1}\left(\frac{c_{root} - c_{tip}}{b/2}\right) \tag{2}$$

while $c_{root}, c_{tip}, \bar{\Lambda}$ and b are the root chord, tip chord, sweep angle calculated and spanwise length geometry parameters (see Fig. 4 in [1]). Additionally, the total rearward sweep angle is dependent on y coordinate only. As a result, the angle calculation was based on simple triangle calculation. From here, Finite wing theory will be brought about by the current context. Note that calculation was performed according to Fig. 1 around the theoretical point – wing apex (0, 0).

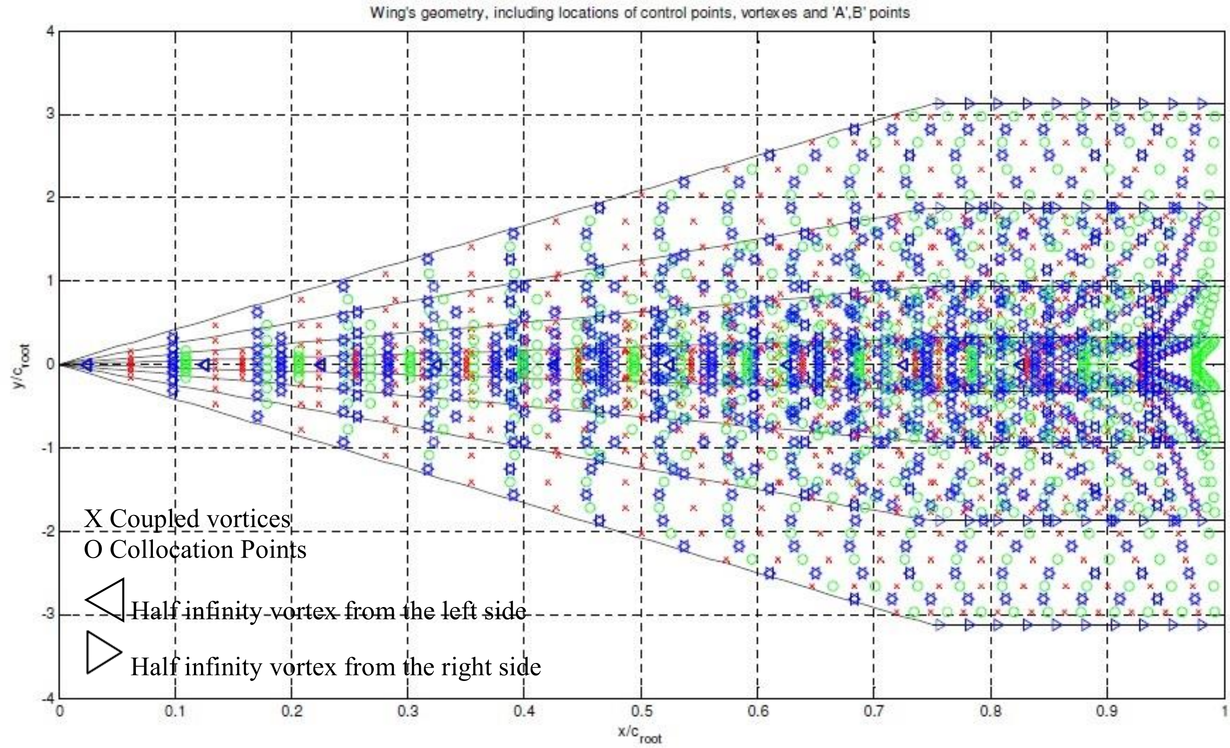

Fig. 1 Extension wing with vortex and

collocation points partition

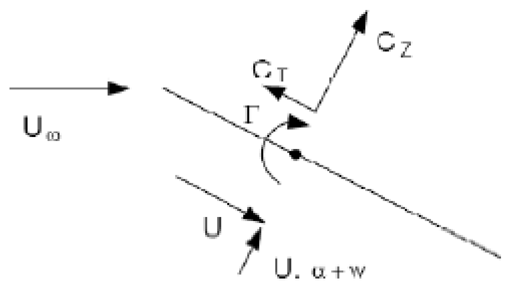

Fig. 2 Description of cross flow and induced velocity including suction force.

3 Finite wing and slender body theories

In the first step, finite-wing theory assumptions which are based on lifting line theory are presented in [1]. However, lift-curve slope in case of swept wing is given by Kuchemann [20]:

$$C_{L_\alpha}\Big|_{\text{Finite-Wing}} \approx \frac{2\pi\cos\Lambda}{1+\dfrac{2\cos\Lambda}{\pi AR}} \qquad (3)$$

According to the slender-body theory [21]:

$$C_{L_\alpha}\Big|_{\text{Slender-Body}} = \frac{\pi AR}{2} \qquad (4)$$

We will also define the errors, such as:

$$\varepsilon_1 = \left|\frac{C_{L\alpha_{\text{finite}}} - C_{L\alpha}}{C_{L\alpha}}\right|, \varepsilon_2 = \left|\frac{C_{L\alpha_{\text{slender}}} - C_{L\alpha}}{C_{L\alpha}}\right| \qquad (5)$$

which present the lifting coefficient errors for the finite wing (ε_1) and slender body (ε_2) theories, respectively.

The center of pressure of the finite wing and slender body theories will be calculated by:

$$X_{Cp}\Big|_{\text{finite}} = \frac{\bar{c}}{4}; \quad X_{Cp}\Big|_{\text{slender}} = \frac{2}{3}\left(c_{root} - c_{tip}\right) \qquad (6)$$

Here, the difference value $c_{root} - c_{tip}$ for all wing configurations will be equal to 0.75. Thus, the center of pressure will be calculated in relative to the average aerodynamic chord (X_{Cp1}) and the wing root chord (X_{Cp2}).

The induced drag coefficient will be calculated for the finite wing theory by the following form:

$$C_{Di}\Big|_{\text{Finite-Wing}} = C_{L_{\text{finite}}} \cdot \alpha_i \underset{\text{Elliptic distribution}}{=} \frac{\left(C_{L\alpha_{\text{finite}}} \cdot \alpha\right)^2}{\pi AR} \qquad (7)$$

In similar way, the slender body induced drag will be:

$$C_{Di}\Big|_{\text{slender}} = C_{L_{\text{slender}}} \cdot \frac{\alpha}{2} \underset{\text{Elliptic distribution}}{=} \frac{\left(C_{L\alpha_{\text{slender}}} \cdot \alpha\right)^2}{\pi AR} \qquad (8)$$

while the induced drag errors for both theories will be defined as:

$$\varepsilon_1 = \left|\frac{C_{D_{\text{finite}}} - C_{Di}}{C_{Di}}\right|, \varepsilon_2 = \left|\frac{C_{D_{\text{slender}}} - C_{Di}}{C_{Di}}\right| \qquad (9)$$

Next section, final results and comparison to finite-wing and slender body theories will be presented and discussed.

4 Results & Discussion

Comparisons between VLM specific aerodynamics parameters for different aspect ratio values, Finite-Wing and Slender body theories are presented in Table 1 alongside Figs. 3-5.

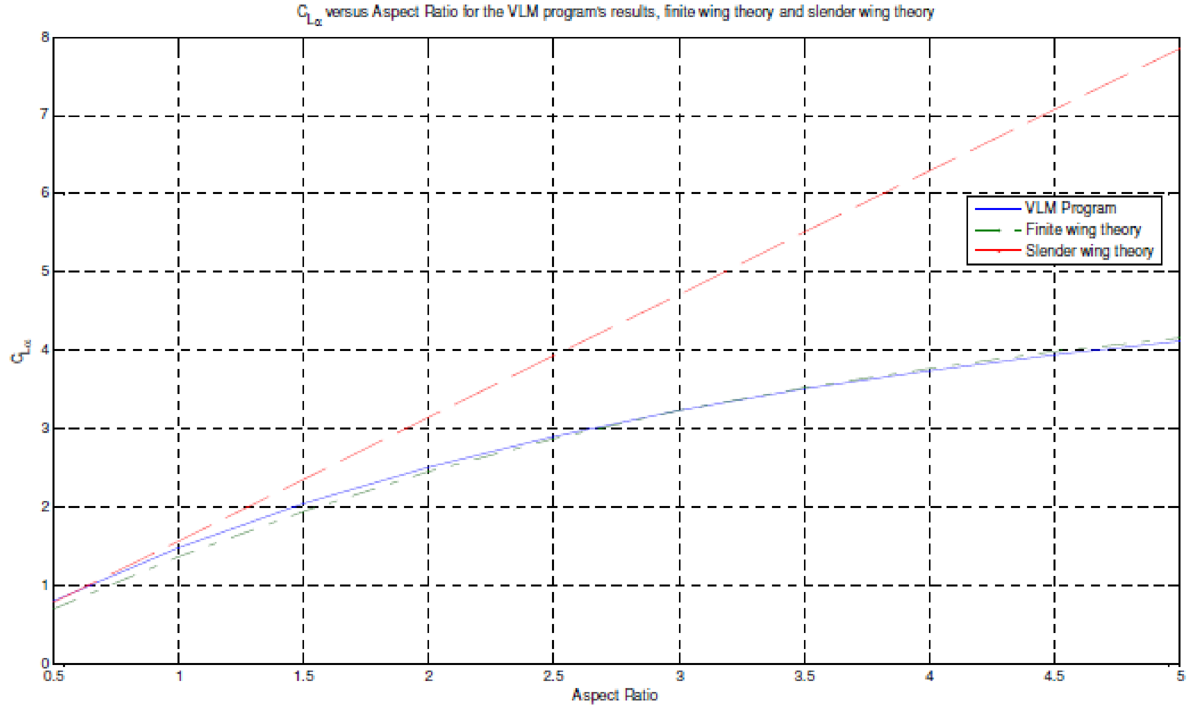

Fig. 3 Lifting coefficients comparison for different AR values: VLM calculation vs. Finite wing and Slender Body theories.

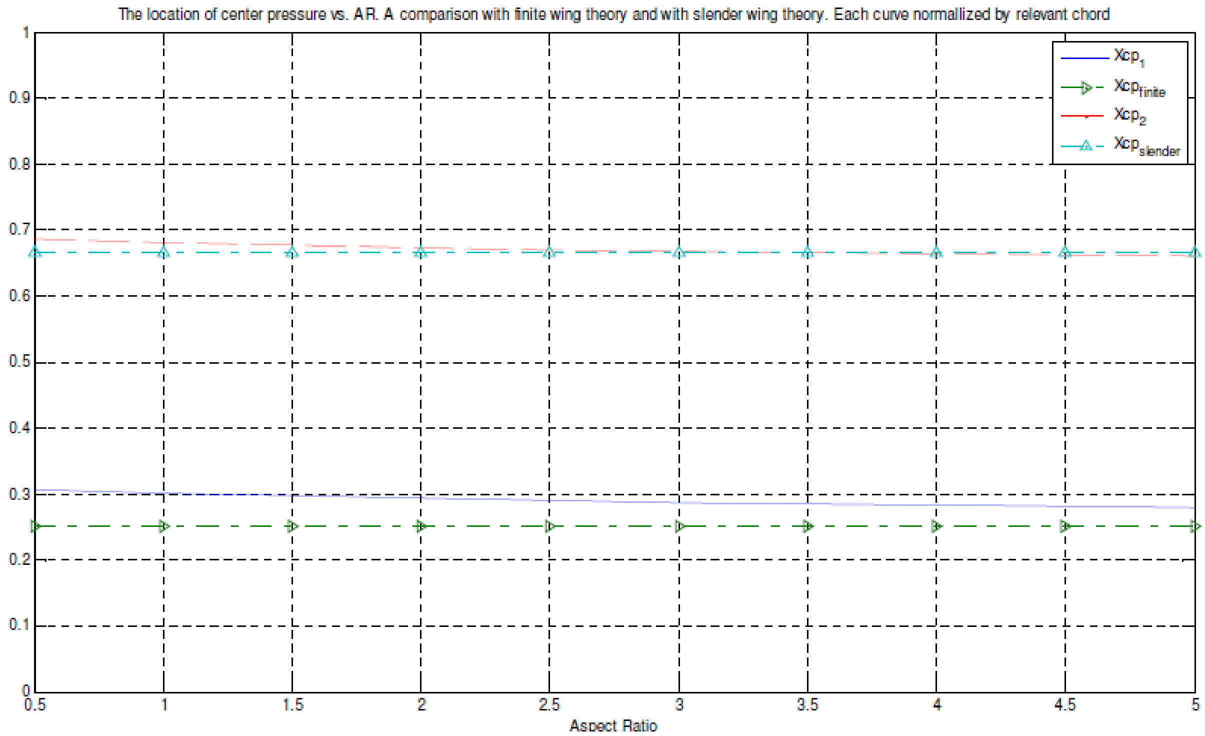

Fig. 4 Center of pressure location comparison for different AR values: VLM calculation vs. Finite wing and Slender Body theories.

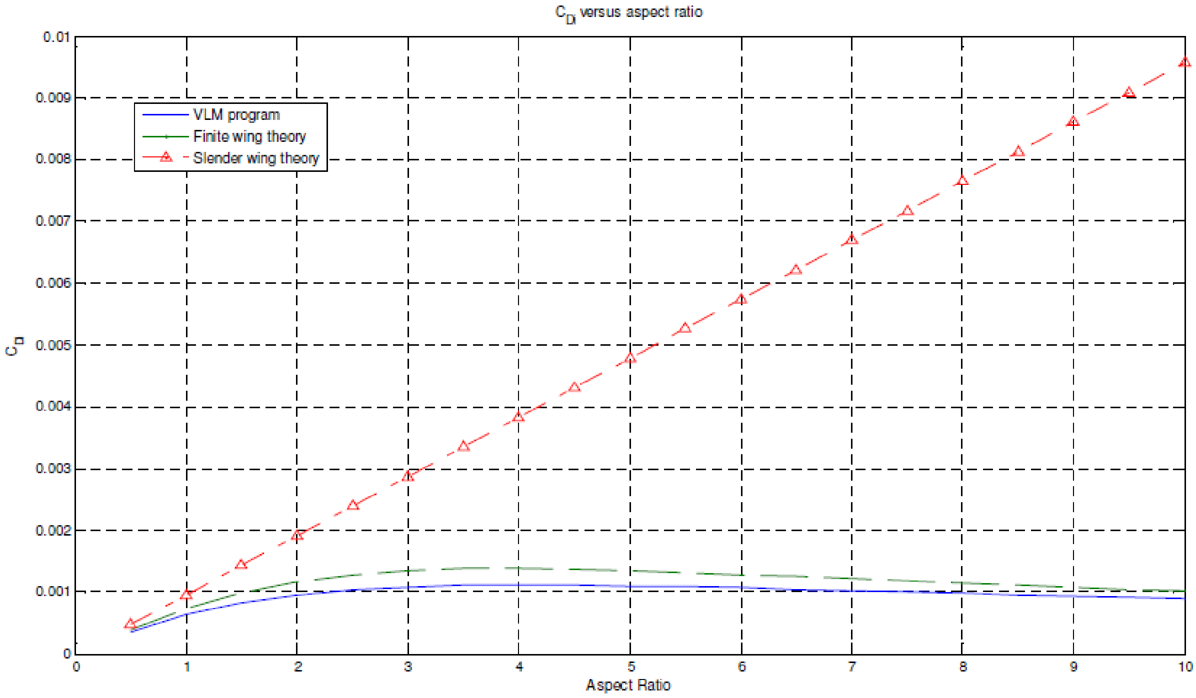

Fig. 5 Induced drag comparison for different AR values: VLM calculation vs. Finite wing and Slender Body theories.

Table 1. Aerodynamics parameter comparisons between VLM, Finite-Wing and Slender body theories.

AR	1	3	6	10
Λ [deg]	67.38014	38.65981	21.80141	13.49573
C_{L_α}	1.47979	3.229202	4.395458	5.057521
$C_{L_{\alpha finite}}$	1.36591	3.226628	4.455002	5.114948
$C_{L_{\alpha slender}}$	1.570796	4.712389	9.424778	15.70796
ϵ_1 [%]	7.695724	0.079709	1.354674	1.135478
ϵ_2 [%]	6.149917	45.93045	114.4208	210.5862
X_{cp_1}	0.300351	0.284992	0.277076	0.272115
X_{cp_2}	0.680287	0.665952	0.658562	0.653932
ϵ_1 [%]	16.76393	12.27833	9.771957	8.127103
ϵ_2 [%]	2.002143	0.107355	1.230589	1.947361
C_{D_i}	0.000638	0.001082	0.001069	0.000888
$C_{D_{i finite}}$	0.000724	0.001346	0.001283	0.001015
$C_{D_{i slender}}$	0.000957	0.002871	0.005742	0.00957
ϵ_1 [%]	13.38276	24.4304	20.06783	14.22796
ϵ_2 [%]	49.9487	165.4061	437.3695	977.283

Examining Table 1 alongside with Figs. 3-5 leads to the following comprehensions about VLM obtained results compared to the finite-wing and slender body theories. One might observe that for AR ~1, the VLM lifting coefficient calculated value becomes closer to the slender body theory, whereas for exceeding ARs value (>1) becomes closer to finite wing theory (Fig. 3). In addition, for relatively high ARs, the VLM center of pressure location value becomes closer to the Finite-Wing theory, whereas the comparison with the slender body theory is unclear (Fig. 4). Finally, it was revealed that for relatively high ARs, the VLM induced drag calculated value becomes closer to the Finite-Wing theory parameter value, whereas the error between the slender body theory and VLM is relatively increasingly high (Fig. 5).

5 Conclusion

In this study we have calculated numerically (improved VLM model) the aerodynamics properties (Lifting & drag coefficients, pressure central location) of Trapeze wing shape Nconfigurations for different aspect ratio values, compared with finite-wing and slender body theories. The wing was divided into planar trapezoid shape panels of the size: 6X6. As expected, for high ARs the VLM solution for the lifting coefficient was coincided with the finite wing theory whereas for small ARs (<1) it was coincided with the slender body theory (~1). Afterwards, we obtained that the calculated VLM induced drag had become closer to the finite-wing theory as the AR value was increasing.

Acknowledgements

This study was performed using Dr. Jose Meyer *Aerodynamics of wings and bodies* course notes from Technion – Israel Institute of Technology and RAFAEL Company. Also, I would like to thank my colleague Mr. Nitai Stein from RAFAEL Company for his assistant the numerical and analytic method presented in this study.

References

[1] Nagler J., (2018) On Boeing 737 – 300 wing aerodynamics calculations based on VLM theory, *Frontiers of Mechatronical Engineering*, **1**, 1-7.

[2] Polhamus E.C., (1966) *A concept of the vortex lift of sharp-edged delta wings based on a leading-edge suction analogy*, NASA TN D-3767.

[3] Polhamus, E.C. (1971) Predictions of vortex-lift characteristics by a leading-edge suction analogy, *AIAA J. Aircraft*, **8**, 4, 193–199.

[4] Traub L. W., (1997) Prediction of Delta Wing Leading-Edge Vortex Circulation and Lift-Curve Slope, *Journal of Aircraft*, **34**, 3, 450-452.

[5] Luckring J. M., (2010) A Survey of Factors Affecting Blunt-Leading-Edge Separation for Swept and Semi-Slender Wings, *ARC: Session: APA-30: Fluid Dynamic Challenges in Flight Mechanics*, 1-34.

[6] A. Shahzad, F. B. Tian, J. Young, and J. C. S. Lai, (2016) Effects of wing shape, aspect ratio and deviation angle on aerodynamic performance of flapping wings in hover, Phys. Fluids 28 (11), 111901.

[7] Yahyaoui M., (2014) Generalized Vortex Lattice Method for Predicting Characteristics of Wings with Flap and Aileron Deflection, *World Academy of Science*, *Engineering and Technology International Journal of Aerospace and Mechanical Engineering*, **8**, 10, 1690-1698.

[8] Nabawy Mostafa R. A., and Crowther William J., (2017) The role of the leading edge vortex in lift augmentation of steadily revolving wings: a change in perspective, *J. R. Soc. Interface*, 14, 1-9.

[9] Ashwin Kumar B., Kumar P., Das S., and Prasad J., (2018) Effect of leading edge shapes on 81°/45° double-delta wing at low speeds. *Proceedings of the Institution of Mechanical Engineers, Part G: Journal of Aerospace Engineering*, 232(16), 3100–3107.

[10] Kaygan E., Ulusoy C., (2018) Effectiveness of Twist Morphing Wing on Aerodynamic Performance and Control of an Aircraft, *Journal of Aviation*, **2**, 2, 77-87.

[11] Traub L. W., (2018) Extending the Leading-Edge Suction Analogy to Nonslender Delta Wings, *Journal of Aircraft*, **55**, 5, 1-4.

[12] Anada G. K., Sukumar P. P., and Selig M. S., (2012) Low-to-Moderate Aspect Ratio Wings Tested at Low Reynolds Numbers, *30th AIAA Applied Aerodynamics Conference*, New Orleans, 1-19.

[13] Lamar J., (2012) A career in vortices and edge forces, *The Aeronautical Journal*, **116**, 1176, 101-152.

[14] Pinzón S., (2015) Introduction to Vortex Lattice Theory. *Ciencia Y Poder Aéreo*, **10**, 1, 39-48.

[15] Boutet J., and Dimitriadis G., (2018) Unsteady Lifting Line Theory Using the Wagner Function for the Aerodynamic and Aeroelastic Modeling of 3D Wings, *Aerospace*, **5**,3, 92.

[16] Luckring J. M., (2019) The discovery and prediction of vortex flow aerodynamics, *The Aeronautical J.*, **123**, 1264, 729-803.

[17] Katz J., and Plotkin A., (2001) Low-Speed Aerodynamics, 2^{nd} Ed., *Cambridge University Press*, Cambridge.

[18] Moran J., (1984) *An Introduction to theoretical and computational aerodynamics*, John Wiley & Sons, New York.
[19] Margason R.J., and Lamar J.E., (1971) *Vortex Lattice Fortran Program for Estimating Subsonic Aerodynamics Characteristics of Complex Planforms*, NASA TN D 6142.
[20] Küchemann D., (1978) The Aerodynamic Design of Aircraft, *Pergamon Press*, Oxford.
[21] Anderson Jr J.D., (1991) Fundamentals of Aerodynamics. 2nd Ed., *McGraw-Hill Inc*.

Contribution of individual authors to the creation of a scientific article (ghostwriting policy)

Author Contributions: The author' own fully creation.

A. Follow: www.wseas.org/multimedia/contributor-role-instruction.pdf

Data Availability

All data, models, and code generated or used during the study appear in the submitted article.

No Interest Conflict

6 The corresponding author (Jacob Nagler) states that there is no conflict of interest.

Sources of funding for research presented in a scientific article or scientific article itself

No funding is involved.

B. Creative Commons Attribution License 4.0 (Attribution 4.0 International , CC BY 4.0)

This article is published under the terms of the Creative Commons Attribution License 4.0
https://creativecommons.org/licenses/by/4.0/deed.en_US